Research paper

Extraction of the sub-band gap density of states of Nb doped ZnO thin film transistors using *C-V* measurements

A. Shaw [a],*, J.D. Jin [a], I.Z. Mitrovic [a], S. Hall [a], J.S. Wrench [b], P.R. Chalker [b]

[a] *Department of Electrical Engineering and Electronic, University of Liverpool, L69 3GJ, United Kingdom*
[b] *Centre for Advanced Materials, University of Liverpool, L69 3GH, United Kingdom*

ARTICLE INFO

ABSTRACT

The sub-band gap density of states (DOS) of Nb doped ZnO thin film transistors were extracted using a multi-frequency capacitance-voltage (*C-V*) method. The results can be represented by a two-term exponential DOS, representing the tail and deep states. The parameters for the tail and deep states are $N_{tail} = 1.6 \times 10^{19}$ cm^{-3}, $T_{tail} = 540$ K, $N_{deep} = 6.5 \times 10^{16}$ cm^{-3} and $T_{deep} = 4058$ K respectively. Furthermore, the DOS from *C-V* provides a good fit with current-voltage characteristics, using the multiple trap and release model.

1. Introduction

Zinc oxide (ZnO) based materials for active channel layers in thin-film transistors (TFTs) have attracted considerable attention for flat panel display applications due to their excellent optical and electrical properties compared to those of Si-based TFTs [1,2]. The carrier concentration in the active channel layer is required in determining the electrical characteristics of the TFTs. The carrier concentration in ZnO is highly dependent on the deposition technique and conditions [3]. Another alternative approach is to add dopants such as Ga and In [4,5], Si [6] or as demonstrated in our previous work, Nb [7] and Mg [8]. The sub-band gap density of states (DOS), $g(E)$, is a key parameter for characterizing ZnO films and a number of techniques have been reported for their extraction. A numerical simulation technique was demonstrated by Kimura et al. [9] where the influence of the free carrier density was assumed negligible. Bae et al. [10] analyzed the variation in the sub-threshold slope in TFTs. The optical response of the DOS has been investigated in both capacitance-voltage (*C-V*) [11,12] and current-voltage (*I-V*) measurements [13]. A method based on multi-frequency *C-V* measurements has been outlined by Lee et al. [14] and Jang et al. [15] based on analysis of the frequency dispersion of *C-V* characteristics, to obtain a frequency-independent plot. Moreover, an extraction technique for the activation energy (E_a) based on the Meyer-Neldel rule was reported by Chen et al. [16] and Jeong et al. [17]. However, this method requires the temperature dependence of the *I-V* characteristics.

Here, we extract the DOS in Nb doped ZnO (ZnO:Nb) TFTs using the multi-frequency *C-V* method outlined by Lee et al. [14] and Jang et al. [15]. This method is based on the derivation of an equivalent circuit for localized and free charge. The advantages of the technique are that optical illumination, temperature-dependent electrical characterization and numerical calculations are not required. The DOS parameters obtained from the *C-V* characteristics are compared with those extracted from *I-V* measurements, which were analyzed using the multi-trapping and release (MTR) model [18] allowing for a self-consistent check of the validity of the results.

2. Experimental

A cross-sectional diagram of the ZnO:Nb TFT is shown in the inset of Fig. 1. Highly doped n-type silicon with a 50 nm thermally oxidized SiO$_2$ layer was used as the substrate. Initially, a 5 nm Al$_2$O$_3$ capping layer was deposited on the SiO$_2$ layer by atomic layer deposition (ALD) at 175 °C. We have found that this provides for a better interface and greatly reduces leakage current in the gate oxide. Without breaking the vacuum, ZnO:Nb was subsequently deposited by ALD at 175 °C to a thickness ($t_{ZnO:Nb}$) of 50 nm using diethylzinc, niobium pentaethoxide and DI water as the precursors for Zn, Nb and the oxidant respectively. The cycle percentage between the Nb and Zn precursor was set to 3.8% corresponding to the optimal *I-V* characteristics in the study of reference [7]. Al source and drain contacts were thermally evaporated with a thickness of 70 nm and patterned using the lift-off process. Each device was isolated by photolithography and wet etching the ZnO:Nb films using an acetic acid solution. Low concentration of acetic acid solution

* Corresponding author.
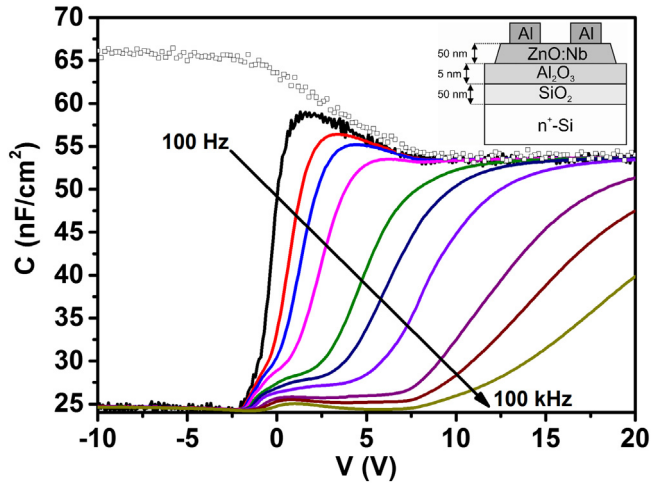*E-mail address:* ee0u92b9@liv.ac.uk (A. Shaw).

Fig. 1. C-V measurements for the substrate (symbols) and 175 °C 3.5% ZnO:Nb TFT (lines) for frequencies between 100 Hz and 100 kHz. The inset shows a schematic of the fabricated TFTs.

(1% in volume) was adopted here with a reasonable etch time of 30 s [7]. Finally, prior to measurements, the devices were annealed at 300 °C in air for 1 h to further reduce the conductivity of the films.

The C-V measurements were conducted in parallel mode using an Agilent E4980A LCR meter under dark conditions. The source and drain contacts were grounded and the ac-signal was applied to the back gate of the device. The frequency (f) was varied in the range of 100 Hz to 100 kHz.

3. Results and discussion

Fig. 1 shows the C-V characteristics with the substrate capacitance (C_{gate}) superimposed and shown with symbols. The substrate capacitance refers to a measurement taken with a metal electrode directly on the gate oxide, to the underlying n$^+$Si. For a negative bias, an accumulation layer is induced at the oxide-Si interface and the ZnO:Nb is depleted; the opposite occurs for a positive bias. Large frequency dispersion is evident for the region of accumulation in the ZnO:Nb film ($V > 0$) and is attributed to capture-emission events occurring in the bulk of the disordered ZnO:Nb film, at the interface with the oxide together with a contribution from series resistance [6]. The bulk response is represented by effective localized (Q_{loc}) and free carrier (Q_{free}) states associated with the ZnO film which is considered to dominate the response.

The donor density (N_d) of the substrate was estimated from the maximum and minimum capacitance in the conventional manner. Using Fig. 1, the depletion capacitance for the substrate is 290 nF/cm^2 and results in a doping concentration of 2.5×10^{18} cm^{-3}, which is consistent with the as-received substrate resistivity. The substrate C-V plot was found to be independent of frequency with a low density of interface states at the thermally grown SiO$_2$/Si substrate interface. For clarity, a parameter C_{gate} is used below to represent the effective gate oxide capacitance for the response of the ZnO film; that is, $C_{gate}(V) = C_{sub}(V)$.

The equivalent circuit associated with the analysis is shown in Fig. 2(a-i). The total impedance of the two-component model (Z_2) is given by

$$Z_2 = \frac{R_m}{1 + (\omega C_m R_m)^2} - j\frac{\omega C_m R_m^2}{1 + (\omega C_m R_m)^2} \tag{1}$$

where $\omega = 2\pi f$, C_m and R_m are the measured capacitance and resistance respectively. The two-component impedance model can be

transformed into the four-component (Z_4) model shown in Fig. 2(a-ii). The four-component model separates the channel impedance and the contact resistances for source and drain (R_s). The impedance of the four-component model is represented as

$$Z_4 = R_s + \frac{R_{ch}}{1 + (\omega C_{ch} R_{ch})^2} - j\left(\frac{\omega C_{ch} R_{ch}}{1 + (\omega C_{ch} R_{ch})^2} + \frac{1}{\omega C_{gate}}\right) \tag{2}$$

where C_{ch} and R_{ch} are the channel capacitance and resistance respectively. It should be noted that the measured leakage current through the gate oxide is <30 pA over the full voltage range and the contact resistances for R_s are assumed to be frequency independent. The voltage dependent R_s is thus extracted and shown in Fig. 2(b). The inset in Fig. 2(b) demonstrates that R_s is determined by the minimum impedance for each applied voltage.

By assuming $Z_2 = Z_4$, the parameters C_{ch} and R_{ch} are obtained using

$$C_{ch} = \frac{bC_{gate}^2 - b^2 C_{gate}}{\left[(ab\omega)^2 + 1\right]C_{gate}^2 - 2bC_{gate} + b^2} \tag{3}$$

where $a = \left(\frac{D_m}{\omega C_m(1+D_m^2)} - R_s\right)$, $b = C_m(1 + D_m^2)$, and $D_m = \frac{1}{\omega C_m R_m}$

$$R_{ch} = \sqrt{\frac{C_m\left(1 + D_m^2\right) - C_{gate}}{\omega^2 C_{ch} C_{gate} - \omega^2 C_{ch} C_m\left(1 + D_m^2\right)C_{ch} + C_{gate}}} \tag{4}$$

The channel impedance, Z_{ch} is represented by

$$Z_{ch} = \frac{R_{ch}}{1 + (\omega C_{ch} R_{ch})^2} - j\frac{\omega C_{ch} R_{ch}^2}{1 + (\omega C_{ch} R_{ch})^2} \tag{5}$$
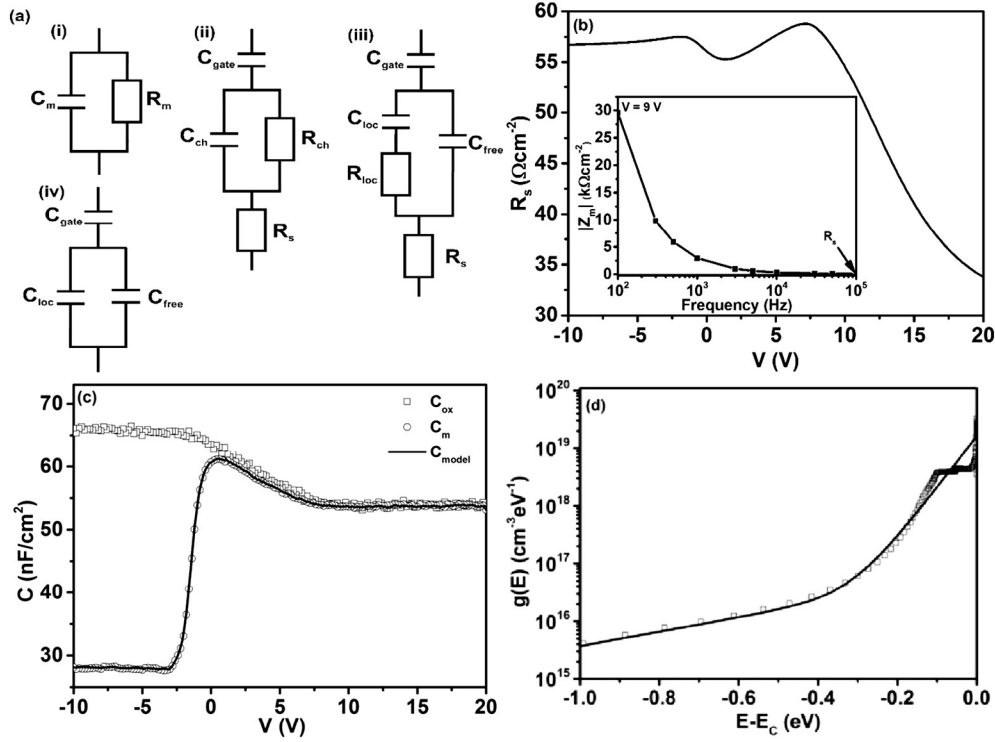
The four-component capacitance model is then transformed into the physics based model, where the channel charge is expressed Q_{loc} and Q_{free} charges. Fig. 2(a-iii) shows the equivalent circuit where C_{loc} is the capacitance dependent on the voltage dependent Q_{loc} and R_{loc} is the equivalent resistance, and C_{free} is the capacitance due to the voltage dependent Q_{free}. The total impedance for the physics based model (Z_{phys}) is then

$$Z_{phys} = \frac{C_{loc}^2 R_{loc}}{\omega^2 C_{loc}^2 R_{loc}^2 + (C_{loc} + C_{free})^2} - j\frac{\omega^2 C_{loc}^2 C_{free} R_{loc}^2 + (C_{loc} + C_{free})}{\omega^3 C_{loc}^2 C_{free}^2 R_{loc}^2 + \omega(C_{loc} + C_{free})^2} \tag{6}$$

where it is assumed that R_{loc} and C_{loc} are frequency independent as their product determines the frequency dependence of Q_{loc}. By using the relationship $Z_{ch} = Z_{phys}$, Eq. (6) can be solved and equated for R_{loc} at the three measured frequencies. The resultant parameters C_{loc}, C_{free}, and R_{loc} obtained are frequency independent. By equating R_{loc} with 3 frequencies such that $R_{loc}(f1) = R_{loc}(f2) = R_{loc}(f3)$, the obtained C_{loc}, C_{free} and R_{loc} are frequency independent. The frequency independent model for the gate capacitance is shown in Fig. 2(a-iv), with the C-V characteristics for this model depicted in Fig. 2(c); the model is seen to overlap the measured characteristics indicating excellent agreement. The frequencies used to obtain Fig. 2(c) are 100 Hz, 10 kHz and 100 kHz; a relatively wide range.

$$R_{loc} = \sqrt{\frac{\omega^2 C_{ch} R_{ch}^2\left(C_{loc} + C_{free}\right)\left(C_{loc} + C_{free} - C_{ch}\right) - \left(C_{loc} + C_{free}\right)}{\omega^2 C_{loc}^2 C_{free}\left[1 + \omega^2 C_{ch} R_{ch}^2\left(C_{ch} - C_{free}\right)\right]}} \tag{7}$$

The procedure associated with Eqs. (1)–(7) has involved the conversion of the frequency dependent C-V plots of Fig. 1, to frequency independent C-V characteristics by employing the equivalent circuit in Fig. 2(a-iv). The resultant C-V characteristics are shown in Fig. 2(c), where

Fig. 2. (a) i. two-component capacitance model for parallel mode measurement, ii. four-component capacitance model for extraction of R_s and the channel impedance, iii. Physics based capacitance model for extracting the C_{loc}, R_{loc} and C_{free} and iv. frequency independent model for the gate capacitance (b) extracted voltage dependent R_s, (c) frequency independent C-V characteristics extracted from three frequencies (f_1 = 100 Hz, f_2 = 10 kHz and f_3 = 100 kHz) and (d) the sub-band gap DOS (symbols) and two-term exponential DOS approximation superimposed (lines). The inset of (b) demonstrates the extraction technique for R_s.

it is evident that the model shows excellent agreement with the measured data. As C_{loc} represents the voltage dependence of Q_{loc}, the DOS, $g(E)$ with units $eV^{-1} cm^{-3}$, is obtained using

$$g(E) = \frac{C_{loc}(V_1) - C_{loc}(V_2)}{q^2 t_{ZnO:Nb}} \qquad (8)$$

Finally, a relationship between the applied voltage on the gate and the surface potential (ϕ_s) is required. The ϕ_s is obtained by integrating the frequency independent C-V characteristics between flat band voltage (V_{FB}) and V shown by

$$\phi_s = \int_{V_{FB}}^{V} \left(1 - \frac{C}{C_{gate}}\right) dV \qquad (9)$$

where V_{FB} was determined from the fitting of I-V measurements using the MTR model. The value of V_{FB} was slightly adjusted (<5%) to achieve a fit with the DOS derived from a TFT measurement taken on the same material, which is described next.

It is generally considered that the DOS associated with deep and tail states can be described by Gaussian distributions. Furthermore, it has been found that those can be approximated by exponential functions representing the tail of the Gaussian in an energy range most populated by carriers [18]. It is also worth noting that it has been recognised and demonstrated that the tail states alone dominate the response [18] and the DOS can be reasonably approximated by a single exponential term, thus allowing a closed form expression for the drain current of a ZnO:Nb TFT. The extracted $g(E)$ (symbols) is shown in Fig. 2(d) with the two-term exponential DOS model superimposed (lines) to account for the tail and deep states given as

$$g(E) = N_{tail} exp\left(-\frac{E_C - E}{kT_{tail}}\right) + N_{deep} exp\left(-\frac{E_C - E}{kT_{deep}}\right) \qquad (10)$$

where N_{tail} is the effective density of tail states, and T_{tail} is the characteristic temperature of tail, N_{deep} is the effective density of deep states, T_{deep} is the characteristic energy of deep states and E_c is the energy of the conduction band. By fitting Eq. (10), the parameters obtained are $N_{tail} = 1.6 \times 10^{19}$ cm^{-3}, $T_{tail} = 540$ K (49 meV), $N_{deep} = 6.5 \times 10^{16}$ cm^{-3} and $T_{deep} = 4058$ K (350 meV).

A comparison of these results from the multi-frequency extraction technique is now made with the DOS obtained from fitting the MTR model to I-V data [7]. The measured I-V characteristics (symbols) and fits from the MTR (lines) and C-V measurements (dashes) are shown in Fig. 3. The I-V fits employ the MTR model with a single exponential DOS approximation, using a characteristic temperature, $T_o = 540$ K
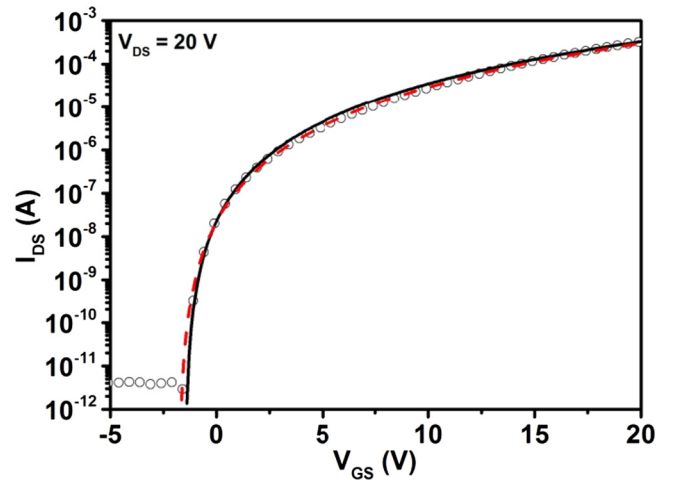
Fig. 3. Transfer characteristics of measured ZnO:Nb TFT (symbols) with W/L = 400 μm/40 μm and fittings using the MTR model (lines) and DOS extracted from the multi-frequency C-V measurements (dashes) [7].

(49 meV) and trap density, $N_t = 1 \times 10^{19} \, cm^{-3}$. It is evident that there is good agreement with the number of trapping states ($N_t \sim N_{tail}$) and the characteristic temperatures ($T_o \sim T_{tail}$), demonstrating the dominance of the tail states on the conduction mechanism.

It should be noted that it is not apparent from the experimental C-V plots of Fig. 1 that the response has become independent of frequency and this implies there may be an associated error in the energy scale for the extracted DOS. The DOS extracted is therefore representative of those states probed in the measurement. The self-consistency between the DOS extracted from C-V and I-V techniques provides some confidence that the results can be used in the construction of a compact device model, as described in [18], which is the ultimate motivation for the work.

4. Conclusions

C-V measurements were conducted on ZnO:Nb TFTs over a frequency range from 100 to 100 k Hz. The tail and deep state density of states were extracted using the multi-frequency method. The tail state DOS component was compared with that extracted from I-V measurements using the MTR model and good agreement found between the two extraction techniques with the qualification that it was necessary to adjust the C-V flat band voltage by <5% to realise the fit.

Acknowledgements

References

[1] S.H.K. Park, C.S. Hwang, M. Ryu, S. Yang, C. Byun, J. Shin, J.I. Lee, K. Lee, M.S. Oh, S. Im, Transparent and photo-stable ZnO thin-film transistors to drive an active matrix organic-light-emitting-diode display panel, Adv. Mater. 21 (2009) 678–682.

[2] X. Yu, T.J. Marks, A. Facchetti, Metal oxides for optoelectronic applications, Nat. Mater. 15 (2016) 383–396.

[3] M.A. Thomas, J.B. Cui, Highly tunable electrical properties in undoped ZnO grown by plasma enhanced thermal-atomic layer deposition, ACS Appl. Mater. Interfaces 4 (2012) 3122–3128.

[4] H. Hosono, Ionic amorphous oxide semiconductors: material design, carrier transport, and device application, J. Non-Cryst. Solids 352 (2006) 851–858.

[5] K. Nomura, A. Takagi, T. Kamiya, H. Ohta, M. Hirano, H. Hosono, Amorphous oxide semiconductors for high-performance flexible thin-film transistors, Jpn. J. Appl. Phys. 45 (2006) 4303.

[6] A.K. Das, P. Misra, L.M. Kukreja, Effect of Si doping on electrical and optical properties of ZnO thin films grown by sequential pulsed laser deposition, J. Phys. D. Appl. Phys. 42 (2009) 165405.

[7] A. Shaw, J.S. Wrench, J.D. Jin, T.J. Whittles, I.Z. Mitrovic, M. Raja, V.R. Dhanak, P.R. Chalker, S. Hall, Atomic layer deposition of Nb-doped ZnO for thin film transistors, Appl. Phys. Lett. 109 (2016) 222103.

[8] A. Shaw, T.J. Whittles, I.Z. Mitrovic, J.D. Jin, J.S. Wrench, D. Hesp, V.R. Dhanak, P.R. Chalker, S. Hall, 45th European Solid State Device Research Conference (ESSDERC) 2015, 2015 206–209.

[9] M. Kimura, T. Nakanishi, K. Nomura, T. Kamiya, H. Hosono, Trap densities in amorphous-InGaZnO$_4$ thin-film transistors, Appl. Phys. Lett. 92 (2008) 133512.

[10] M. Bae, D. Yun, Y. Kim, D. Kong, H.K. Jeong, W. Kim, J. Kim, I. Hur, D.H. Kim, D.M. Kim, Differential ideality factor technique for extraction of subgap density of states in amorphous InGaZnO thin-film transistors, IEEE Electron Device Lett. 33 (2012) 399–401.

[11] K. Jeon, C. Kim, I. Song, J. Park, S. Kim, S. Kim, Y. Park, J.-H. Park, S. Lee, D.M. Kim, D.H. Kim, Modeling of amorphous InGaZnO thin-film transistors based on the density of states extracted from the optical response of capacitance-voltage characteristics, Appl. Phys. Lett. 93 (2008) 182102.

[12] J.H. Park, K. Jeon, S. Lee, S. Kim, S. Kim, I. Song, C.J. Kim, J. Park, Y. Park, D.M. Kim, D.H. Kim, Extraction of density of states in amorphous GaInZnO thin-film transistors by combining an optical charge pumping and capacitance–voltage characteristics, IEEE Electron Device Lett. 29 (2008) 1292–1295.

[13] H. Bae, H. Seo, S. Jun, H. Choi, J. Ahn, J. Hwang, J. Lee, S. Oh, J.U. Bae, S.J. Choi, D.H. Kim, D.M. Kim, Fully current-based sub-bandgap optoelectronic differential ideality factor technique and extraction of subgap DOS in amorphous semiconductor TFTs, IEEE Trans. Electron Devices 61 (2014) 3566–3569.

[14] S. Lee, S. Park, S. Kim, Y. Jeon, K. Jeon, J.H. Park, J. Park, I. Song, C.J. Kim, Y. Park, D.M. Kim, D.H. Kim, Extraction of subgap density of states in amorphous InGaZnO thin-film transistors by using multifrequency capacitance–voltage characteristics, IEEE Electron Device Lett. 31 (2010) 231–233.

[15] J. Jang, J. Kim, M. Bae, J. Lee, D.M. Kim, D.H. Kim, J. Lee, B.-L. Lee, B. Koo, Y.W. Jin, Extraction of the sub-bandgap density-of-states in polymer thin-film transistors with the multi-frequency capacitance-voltage spectroscopy, Appl. Phys. Lett. 100 (2012) 133506.

[16] C. Chen, K. Abe, H. Kumomi, J. Kanicki, Density of states of a-InGaZnO from temperature-dependent field-effect studies, IEEE Trans. Electron Devices 56 (2009) 1177–1183.

[17] J. Jeong, J.K. Jeong, J.S. Park, Y.G. Mo, Y. Hong, Meyer–Neldel Rule and extraction of density of states in amorphous indium–gallium–zinc-oxide thin-film transistor by considering surface band bending, Jpn. J. Appl. Phys. 49 (2010), 03CB02. .

[18] F. Torricelli, J.R. Meijboom, E. Smits, A.K. Tripathi, M. Ferroni, S. Federici, G.H. Gelinck, L. Colalongo, Z.M. Kovacs-Vajna, D.D. Leeuw, E. Cantatore, Transport physics and device modeling of zinc oxide thin-film transistors part I: long-channel devices, IEEE Trans.Electron Devices 58 (2011) 2610–2619.